Some numerical experiments on the effect of the variation of static stability in two-layer quasi-geostrophic models

By LENNART BENGTSSON, *Institute of Meteorology, University of Stockholm, and Swedish Meteorological and Hydrological Institute*

(Manuscript received June 2, 1964)

ABSTRACT

A method to solve a quasi-geostrophic two-layer model including the variation of static stability is presented. The divergent part of the wind is incorporated by means of an iterative procedure. The procedure is rather fast and the time of computation is only 60–70 % longer than for the usual two-layer model. The method of solution is justified by the conservation of the difference between the gross static stability and the kinetic energy.

To eliminate the side-boundary conditions the experiments have been performed on a zonal channel model.

The investigation falls mainly into three parts:

The first part (section 5) contains a discussion of the significance of some physically inconsistent approximations. It is shown that physical inconsistencies are rather serious and for these inconsistent models which were studied the total kinetic energy increased faster than the gross static stability.

In the next part (section 6) we are studying the effect of a Jacobian difference operator which conserves the total kinetic energy. The use of this operator in two-layer models will give a slight improvement but probably does not have any practical use in short periodic forecasts. It is also shown that the energy-conservative operator will change the wave-speed in an erroneous way if the wave-number or the grid-length is large in the meridional direction.

In the final part (section 7) we investigate the behaviour of baroclinic waves for some different initial states and for two energy-consistent models, one with constant and one with variable static stability. According to the linear theory the waves adjust rather rapidly in such a way that the temperature wave will lag behind the pressure wave independent of the initial configuration. Thus, both models give rise to a baroclinic development even if the initial state is quasi-barotropic.

The effect of the variation of static stability is very small, qualitative differences in the development are only observed during the first 12 hours. For an amplifying wave we will get a stabilization over the troughs and an instabilization over the ridges.

1. Introduction

During the past ten years a great number of simple (two-level or two-parameter) models have been designed for the purposes of numerical weather prediction. Some of these models have also been tested for a long time and under a variety of atmospheric initial data. Some physical shortcomings have been reported by Gates (1961) and they may be repeated here: (1) a tendency to underestimate the growth of relatively new large-scale disturbances, (2) to overestimate the growth of the relatively mature disturbances accompanied by fictitious large gradients, and (3) to display a spurious growth of anticyclonic circulation, especially in the subtropical latitudes.

The most serious and also the most intricate of these errors is the second one, and we will in this study mainly restrict ourselves to this effect. Those who daily follow up forecasts with the simple two-parameter model eq. (2.17–2.18), terms notated A_{mn}, observe that the forecast for the mean level sometimes is inferior to the result from the barotropic, one-parameter model. These circumstances are a painful reality for those involved in routine numerical weather prediction and some have made the drastic decision to neglect the term which controls the effect from the thermal field on the mean field. (Döös (1962) A_{32} in eq. (2.17)). This is the same as to perform barotropic forecasts for the mean level.

Let us discuss this problem somewhat further. What are we doing when we formulate a conventional two-level model? Disregarding the general constraints on the fluid (frictionless, hydrostatic and adiabatic flow) we have two "geometrical" constraints on the forecasting equations. The horizontal wind has a linear variation in the vertical direction, and the vertical wind has a symmetrical distribution around the mean level. This means also that the divergent part of the wind is symmetrically distributed in the vertical.

Our empirical knowledge of a baroclinic development tells us on the other hand that this is quite an erroneous description of what is really happening. The baroclinic development starts as a rule at a special level in the atmosphere and after some time (10–24 hours) the greater part of the troposphere is taking part in the baroclinic development. Simultaneously large variations in the vertical distribution of divergence are observed. Consequently, this last process is not possible to describe with a two-layer model.

In the following experiments we will not be able to justify by an explicit procedure that the constraints on the windfield are the most serious of our assumptions, but we will by a successive elimination of other sources of error find this to be quite plausible.

Another explanation to the systematic error of overprediction of mature disturbances has been discussed by Gates. (1961, 1963). If we allow the static stability to vary in space and time, the release of the kinetic energy of the disturbances is regulated. During the development stage the local conversion of potential energy into kinetic energy may be systematically underestimated (the static stability is small), while during the occlusion and decay stage the potential energy may be overestimated (the static stability is large).

A third source of error may also be due to inconsistent approximations in the forecast equations with respect to the conservation of the total energy.

The errors due to purely mathematical approximations will also be studied and an investigation concerning the significance of the conservation of the kinetic energy in the finite-difference form will be discussed separately in section 6.

In this article we are going to discuss these kinds of error quantitatively by performing some series of numerical experiments. In order to focus our interest on the most important error due to the physical shortcomings of the model we will arrange the experiments in such a way that errors of other kinds are reduced as much as possible. In the experimental models which will be discussed, the motion is confined to a zonal channel consisting of walls to the north and to the south and open boundary to the west and the east.

For the initial data we have taken simple analytical expressions. By doing so we may exclude errors due to inaccurate and non-representative initial data and also errors due to incorrect specification of the boundary condition.

The first part of this article will describe the formulation of a two-layer model with a variable static stability suited for numerical weather prediction. The same model has been investigated by Gates (1963). However, in these experiments we have chosen to solve the system of equations in another way; thus we compute the vertical velocity by the aid of the thermal equation and then the divergent part of the wind is incorporated with the aid of an iterative procedure.

It is shown that only one scan is enough to give a satisfactory result, manifested by the conservation of the difference between the kinetic energy and gross static stability.

The results of the channel experiments will be presented as different area-integrations which will demonstrate the behaviour of baroclinic waves for some consistently and inconsistently formulated forecasting models.

Finally we shall discuss the dynamic manifestations of some wave-solutions for the simple two-level model given in closed form by Ogura (1957) and Wiin-Nielsen (1960). These will be accompanied by similar numerical experiments for the model with constant and variable static stability.

The following notations will be adopted:

x = Cartesian distance coordinate to east
y = Cartesian distance coordinate to north
p = pressure
t = time

$(u,v,w,)$ = time rates of change of (x,y,p) following the motion
$\mathbf{v}$ = horizontal velocity vector
g = acceleration of gravity
$\mathbf{k}$ = vertical unit vector
ξ = vertical vorticity component
ψ = stream function
χ = velocity potential
θ = potential temperature
c_p, c_v = specific heats of air at constant pressure and volume
$R = c_p - c_v$
$\varkappa = R/c_p$

2. The model

A very suitable model for this kind of investigation has been designed by LORENZ (1960). This model has been very generally formulated and we will in this connection only retain those parts of the equations which are energy-consistent, with the balance equation.

The basic equations (in the *xypt*-system) are as follows.

The thermal equation:

$$\frac{\partial \theta}{\partial t} = -\mathbf{v}\cdot\nabla\theta - \omega\frac{\partial\theta}{\partial p}. \tag{2.1}$$

The vorticity equation:

$$\frac{\partial \xi}{\partial t} = -\mathbf{v}\cdot\nabla\eta - \omega\frac{\partial\xi}{\partial p} - \eta\nabla\cdot\mathbf{v} - \mathbf{k}\cdot\left(\nabla\omega\times\frac{\partial\mathbf{v}}{\partial p}\right). \tag{2.2}$$

The continuity equation:

$$\frac{\partial\omega}{\partial p} + \nabla\cdot\mathbf{v} = 0, \tag{2.3}$$

where

$$\mathbf{v} = \mathbf{k}\times\nabla\psi + \nabla\chi,$$

$$\eta = \xi + f$$

Inserting the horizontal wind-field in the equations and omitting the divergent part of the wind in the twisting term γ in the vorticity equation we get:

$$\frac{\partial\theta}{\partial t} = -J(\psi,\theta) - \nabla\chi\cdot\nabla\theta - \omega\frac{\partial\theta}{\partial p}, \tag{2.4}$$

$$\frac{\partial\xi}{\partial t} = -J(\psi,\eta) - \nabla\chi\cdot\nabla\eta - \omega\frac{\partial\xi}{\partial p} - (\xi+f)\nabla^2\chi - \nabla\omega\cdot\nabla\frac{\partial\psi}{\partial p}. \tag{2.5}$$

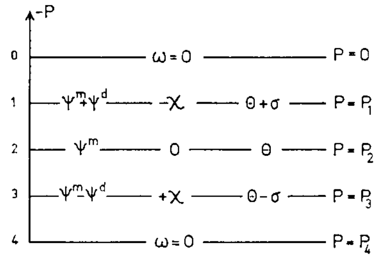

FIG. 1. The information levels, and primary dependent variables of the two-layer model under investigation.

If we apply the eqs. (2.4) and (2.5) to a two-layer model of the atmosphere as illustrated in Fig. 1, we obtain the following equations (cf. Lorenz):

$$\frac{\partial\theta}{\partial t} = -A_{11}J(\psi^m,\theta) + A_{12}\frac{\omega}{\Delta p}\sigma - B_{13}J(\psi^d,\sigma) + B_{14}\nabla\sigma\cdot\nabla\chi, \tag{2.6}$$

$$\frac{\partial\sigma}{\sigma t} = -B_{21}J(\psi^m,\sigma) + B_{22}\nabla\theta\cdot\nabla\chi - D_{23}J(\psi^d,\theta), \tag{2.7}$$

$$\nabla^2\frac{\partial\psi^m}{\partial t} = -A_{31}J(\psi^m,\eta^m) - A_{32}J(\psi^d,\xi^d) + D_{33}\xi^d\frac{\omega}{\Delta p} + D_{34}\frac{1}{\Delta p}\nabla\omega\cdot\nabla\psi^d + D_{35}\nabla\xi^d\cdot\nabla\chi + D_{36}\xi^d\frac{\omega}{\Delta p}, \tag{2.8}$$

$$\nabla^2\frac{\partial\psi^d}{\partial t} = -A_{41}J(\psi^m,\xi^d) - A_{42}J(\psi^d,\eta^m) + A_{43}\frac{f\omega}{\Delta p} + B_{44}\nabla f\cdot\nabla\chi + D_{45}\xi^m\frac{\omega}{\nabla p} + D_{46}\nabla\xi^m\cdot\nabla\chi, \tag{2.9}$$

$$2^{-(1+\varkappa)}R\nabla^2\theta = \nabla\cdot(f\nabla\psi^d) + \nabla\{\nabla^2\psi^m\nabla\psi^d + \nabla^2\psi^d\nabla\psi^m - \nabla(\nabla\psi^m\cdot\nabla\psi^d)\}. \tag{2.10}$$

Here $\quad \psi^m = \dfrac{\psi_1+\psi_3}{2}, \quad \psi^d = \dfrac{\psi_1-\psi_3}{2},$

$$\theta = \frac{\theta_1+\theta_3}{2}, \quad \sigma = \frac{\theta_1-\theta_2}{2},$$

and $\quad \chi = \dfrac{\chi_3-\chi_1}{2},$

where the subscripts refer to the levels shown in Fig. 1.

To obtain eqs. (2.6)–(2.9) we have applied the thermodynamic equation and the vorticity equation to both of the levels 1 and 3 and after that we have formed the sum and the difference of the two equations. We have also evaluated vertical finite differences over $\Delta p (p_0 = 1000$ mb in assumed constant), with the vertical boundary conditions $\omega = 0$ at both $p = 0$ and $p = p_0$. The approximations $\theta_2 = (\theta_1 + \theta_3)/2$ have also been used. Eq. (2.10) is derived in the same manner as that by GATES (1961), by differentiating (2.4) with respect to pressure using the hydrostatic relations, and evaluating $\partial\psi/\partial p$ by finite differences over Δp about the level 2. If one introduces the continuity equation of the form:

$$\frac{\omega}{\Delta p} - \nabla^2 \chi = 0 \tag{2.11}$$

it is easy to see that the system of eqs. (2.6)–(2.10) will be just the same as that published by LORENZ (1960) and GATES (1961). ω is the vertical motion at level 2.

The coefficients "A_{mn}", "B_{mn}" and "D_{mn}" appearing in front of every term in the equation are used for identification. The subscript "m" refers to the original equation and the subscript "n" to the specific term. The terms denoted by A_{mn} and B_{mn} are consistent with the quasi-geostrophic equation and the terms denoted by A_{mn}, B_{mn} and D_{mn}, with the complete balance equation.

In particular, eq. (2.8) with term A_{31} is simply the non-divergent barotropic equation and all the terms A_{mn} together with the linear part of equation (2.10) form the ordinary two-parameter model of CHARNEY & PHILLIPS (1953).

This last statement may be clear if we eliminate ω between eqs. (2.6) and (2.9). This procedure gives us the equation:

$$\begin{aligned}\nabla^2 \frac{\partial \psi^d}{\partial t} &= A_{41} J(\xi^d, \psi^m) + A_{42} J(\eta^m, \psi^d) + B_{44} \nabla f \cdot \nabla \chi \\ &+ D_{46} \nabla \xi^m \cdot \nabla \chi + \frac{A_{43} f + D_{45} \xi^m}{A_{12} \sigma} \left\{ \frac{\partial \theta}{\partial t} \right. \\ &+ A_{11} J(\psi^m, \theta) + B_{13} J(\psi^d, \sigma) \\ &\left. + B_{14} \nabla \sigma \cdot \nabla \chi \right\}.\end{aligned} \tag{2.12}$$

The quasi-geostrophic balance for the thermal equation will be introduced in the following way:

$$\nabla \psi^d = \frac{g}{f} \nabla z^d.$$

By the aid of the hydrostatic relation we then get:

$$\nabla \theta = \frac{2^{\varkappa+1}}{R} f \nabla \psi^d. \tag{2.13}$$

If we further assume that the following will hold:

$$\frac{\partial \theta}{\partial t} = \frac{2^{\varkappa+1}}{R} f \frac{\partial \psi^d}{\partial t} \tag{2.14}$$

and introduce the new variables:

$$W = \frac{\omega}{\nabla p}, \tag{2.15}$$

$$s = R 2^{-(1+\varkappa)} \sigma, \tag{2.16}$$

we get the following system of 3 equations (θ has been eliminated by the aid of the quasi-geostrophic assumption):

$$\begin{aligned}\nabla^2 \frac{\partial \psi^m}{\partial t} &= A_{31} J(\eta^m, \psi^m) + A_{32} J(\xi^d, \psi^d) \\ &+ (D_{33} + D_{36}) \xi^d W + D_{34} \nabla W \cdot \nabla \psi^d \\ &+ D_{35} \nabla \xi^d \cdot \nabla \chi,\end{aligned} \tag{2.17}$$

$$\begin{aligned}\left\{ \nabla^2 - \frac{A_{43} f + D_{45} \xi^m}{A_{12} s} \right\} \frac{\partial \psi^d}{\partial t} &= A_{41} J(\xi^d, \psi^m) \\ &+ A_{42} J(\eta^m, \psi^d) + \frac{A_{43} f + D_{45} \xi^m}{A_{12} S} \{ A_{11} f J) \psi^m, \psi^d) \\ &+ B_{13} J(\psi^d, s) + B_{14} \nabla s \cdot \nabla \chi \} \\ &+ B_{44} \nabla f \cdot \nabla \chi + D_{45} \nabla \xi^m \cdot \nabla \chi,\end{aligned} \tag{2.18}$$

$$\frac{\partial s}{\partial t} = B_{21} J(\psi^m, s) + B_{22} f \nabla \psi^d \cdot \nabla \chi. \tag{2.19}$$

To solve the systems (2.17)–(2.19) we must have an expression for χ. With the aid of the continuity equation (2.11), the definition (2.16), the thermal equation (2.6) and the quasi-geostrophic assumption we get the following expression:

$$\nabla^2\chi = \frac{1}{A_{12}s}\left\{\frac{\partial\psi^d}{\partial t} + A_{11}fJ(\psi^m,\psi^d) + B_{13}J(\psi^d,s) - B_{14}\nabla s\cdot\nabla\chi\right\}. \quad (2.20)$$

To illustrate the computational procedure we write the equations in the following way:

$$\left.\begin{aligned}
&\text{(a)}\quad \{\nabla^2 - q(x,y)\}\frac{\partial\psi^{d\nu}}{\partial t} = F_1(\psi^m,\psi^d,s,\chi^\nu)\\
&\text{(b)}\quad \nabla^2\frac{\partial\psi^{m\nu}}{\partial t} = F_2(\psi^m,\psi^d,s,\chi^\nu)\\
&\text{(c)}\quad \frac{\partial s^\nu}{\partial t} = F_3(\psi^m,\psi^d,s,\chi^\nu)\\
&\text{(d)}\quad \nabla^2\chi^{\nu+1} = F_4\left(\psi^m,\frac{\partial\psi^d}{\partial t},s,\chi^\nu\right)
\end{aligned}\right\} \quad (2.21)$$

here (2.21a) corresponds to (2.18); (2.21b); to (2.17); (2.21c) to (2.19) and (2.21d) to (2.20).

The superfix ν here denotes the order of iteration. The initial values are given in ψ^m, ψ^d and σ and the system is solved in the order $a\rightarrow b\rightarrow c\rightarrow d$.

The first guess of χ is zero. The system is thus first solved as an ordinarily two-layer model with constant static stability, combined with the non-divergent term denoted B_{mn} and the equation for the static stability.

The solution of the Poisson eq. (2.21d) gives us the new χ, after which the system (2.21a)–(2.21d) is resolved and attention is paid to the divergent terms. The iterative procedure is in this case very successful and we will in the first scan catch more than 95 % of the velocity-potential field.

With this fast rate of convergence one scan was enough to incorporate the divergent wind-field. The computation time for the system corresponding to the terms notated A_{mn}, B_{mn} therefore only exceeds that of the ordinary two-layer model with 60–70 %. The finite-difference form of the eqs. (2.17)–(2.20) is described in the Appendix.

The systems (2.6)–(2.9) may naturally be solved in many different ways. Another procedure has been described by GATES (1963). He uses the so-called ω-equation, the diagnostic relationship which we get if we eliminate the time-derivatives from the vorticity and the thermal equation. However, this method must be criticized. When we want to obtain analytical solutions to a system of differential equations it may sometimes be useful to reduce the number of equations by increasing the order of the remaining ones.

This method is not to be recommended if we want to solve our equation approximately, by numerical methods. If, as often is the case, we are restricted to a fixed number of adjacent points when we want to truncate a difference operator, the truncation error increases rapidly with the order of the operator. Another problem which arises if we use the ω-equation is that we ought to introduce one artificial constraint on the coriolis parameter if we want to preserve the total mass and on the static stability in order to get convergence in the solution of the ω-equation. For further references see GATES (1963).

In order to check if our method of solution is justified we have found it is naturally required that the system should conserve the difference between the kinetic energy and the gross static stability (cf. LORENZ). If this is true the method of solution and especially the difference scheme is acceptable.

As is seen from Fig. 5, showing the variation of kinetic energy and gross static stability with time, our methods are really justified.

3. Initial data

As the initial situation ($t=0$) we assume a very simple baroclinic basic flow, characterized by a zonal basic current, U^m for the mean field and U^d for the thermal field, independent of the horizontal coordinates. The basic state has further a constant static stability σ.

A disturbance flow is superimposed on the basic initial field in the following way.

Given, at the time $t=0$ sinusoidal disturbances in the mean, thermal and the stability fields in the form of the following expressions:

$$\left.\begin{aligned}
\psi^{m'} &= \psi_A^m \sin\frac{2\pi}{L}x\cos\frac{2\pi}{D}y,\\
\psi^{d'} &= \psi_A^d \sin\frac{2\pi}{L}(x-\gamma^d)\cos\frac{2\pi}{D}y \quad \text{for} \quad |y|\leqslant\frac{D}{2},\\
\sigma' &= \sigma_A \sin\frac{2\pi}{L}(x-\gamma^s)\cos\frac{2\pi}{D}y.
\end{aligned}\right\} \quad (3.1)$$

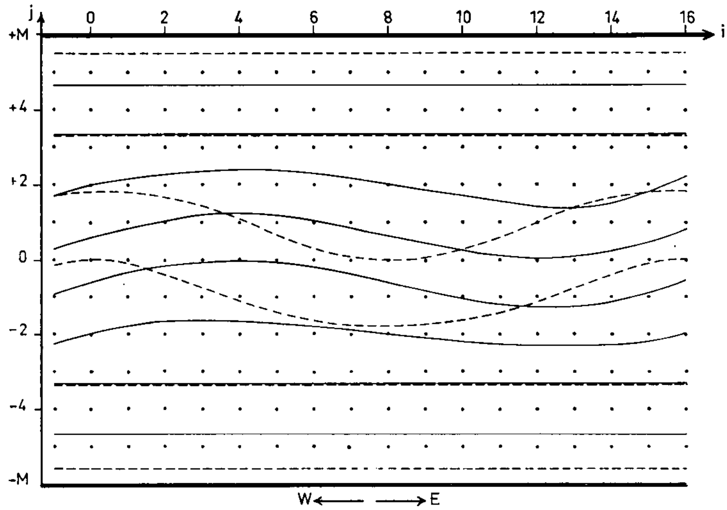

FIG. 3. The channel model with an initial disturbance ($\gamma^d = \frac{1}{2}\pi$). Mean field (solid lines), temperature field (dashed lines).

The amplitudes of the disturbances are denoted by subindex "A", L is the wave-length in the zonal direction, D is the wave-length in the meridional direction, γ^d and γ^s are the phase lags for the temperature wave $\psi^{d'}$ and for the stability wave σ' respectively.

The numerical values which have been used in the computations are specified later.

In the channel experiment we have used the β-plane approximation.

For further description of the channel see Fig. 3.

4. Energy computations

To depict the state of the flow we have computed some energy relationships at every time step. In discussing these relationships, described in the form of area or volume integrals, we will make use of the following notations. Let, as before, α be an arbitrary variable. We then define:

$$\left\{\begin{array}{l}\alpha = \bar{\alpha} + \alpha', \\ \alpha' = \tilde{\alpha} + \alpha'',\end{array}\right\} \tag{4.1}$$

where
$$\bar{\alpha} = \frac{1}{2LM}\int_s \alpha ds \tag{4.2}$$

and
$$\tilde{\alpha} = \frac{1}{L}\int_0^L \alpha dx. \tag{4.3}$$

s represents a closed area, ($s = 2LM$ (see Fig. 3)) and ds is an infinitesimal area element. $\bar{\alpha}$ will be referred to as the area mean and $\tilde{\alpha}$ as the zonal mean. L is the wave-length of the baroclinic disturbance and M is half the width of the channel.

The kinetic energy of the mean zonal flow and of the perturbation flow is expressed in the following way:

$$\tilde{K} = \frac{p_0}{2g}\int_s (\nabla\tilde{\psi}^m \cdot \nabla\tilde{\psi}^m + \nabla\tilde{\psi}^d \cdot \nabla\tilde{\psi}^d) ds, \tag{4.4}$$

$$K'' = \frac{p_0}{2g}\int_s (\nabla\psi^{m''} \cdot \nabla\psi^{m''} + \nabla\psi^{d''} \cdot \nabla\psi^{d''}) ds. \tag{4.5}$$

The total potential energy is given by LORENZ (1960):

$$P + I = \frac{p_0 c_P}{g} a \int_s \theta ds - \frac{p_0 c_P}{g} b \int_s \sigma ds, \tag{4.6}$$

where $a = 0.797$ and $b = 0.124$.

The negative of the second term in (4.6) is the gross static stability:

$$S = \frac{p_0 c_P}{g} b \int_s \sigma ds. \tag{4.7}$$

It follows from eqs. (2.6) and (2.11) that

$$\int_s \frac{\partial \theta}{\partial t} ds = 0$$

which implies that the first integral in (4.6) is a constant. Thus, if the total energy $K+P+I$ were conserved, the difference between S and K would be conserved or vice versa.

In order to make comparisons with the investigation presented by THOMPSON (1959) and also with the quantities,

$$\text{ROT} = \overline{\xi^{m2} + \xi^{d2}} \tag{4.8}$$

and

$$\text{OCC} = \overline{\left(\frac{\xi^m \xi^d}{\xi^{m2} + \xi^{d2}}\right)} \tag{4.9}$$

have been computed. The first integral is a measure of the total rotationality of the flow and the second integral may be regarded as a measure of the state of occlusion. For a more detailed description, reference is made to THOMPSON (1959).

Finally, in order to get a more detailed picture of what will happen to a baroclinic disturbance in a zonal channel we have also computed the kinetic energy of the divergent wind, the available potential energy of the zonal and the perturbation flow, and the energy conversions from the potential energy to the kinetic energy. The expressions for these integrals are:

$$\overleftarrow{K^{\tilde{\chi}}} = \frac{p_0}{2g}\int_s (\nabla\tilde{\chi}\cdot\nabla\tilde{\chi})ds, \tag{4.10}$$

$$K^{\chi''} = \frac{p_0}{2g}\int_s (\nabla\chi''\cdot\nabla\chi'')ds, \tag{4.11}$$

$$\{\tilde{A}\cdot\tilde{K}\} = -\frac{R}{2^{\varkappa}g}\int_s \tilde{\theta}\tilde{\omega}ds, \tag{4.12}$$

$$\{A''\cdot K''\} = -\frac{R}{2^{\varkappa}g}\int_s \theta''\omega''ds, \tag{4.13}$$

$$\tilde{A} = \frac{Rp_0}{2^{\varkappa+1}g}\int_s \frac{\overline{\tilde{\theta}}^2 + \overline{\tilde{\sigma}}^2}{\bar{\sigma}+\bar{\sigma}_{\max}} ds, \tag{4.14}$$

$$A'' = \frac{Rp_0}{2^{\varkappa+1}g}\int_s \frac{\overline{\theta''^2} + \overline{\sigma''^2}}{\bar{\sigma}+\bar{\sigma}_{\max}} ds, \tag{4.15}$$

where $\bar{\sigma}_{\max}$ denotes the maximum value under adiabatic redistribution, LORENZ (1960).

The integral relationship has for comparison been computed for two models, one with constant static stability and the other with variable static stability. The integrals have been approximated by finite sums. Thus, for an arbitrary function $f(xy)$ we have:

$$\int_s f(xy)ds \simeq \sum_{i=0}^{i=L}\sum_{j=-M}^{j=+M} f(xy)_{ij}\Delta A, \tag{4.16}$$

where ΔA corresponds to an elementary grid square.

5. The effect of inconsistent approximations in the differential equation

We will in the following make use of four different models.

Model I: The terms denoted by A_{mn} in eqs. (2.17)–(2.19). Consistent model with respect to energy, inconsistent with respect to vorticity.

Model II: The terms denoted by A_{mn} and B_{mn} in eqs. (2.17)–(2.20). Consistent model with respect to energy, consistent with respect to vorticity.

Model III: The terms denoted by A_{mn}, B_{mn}, D_{33}, D_{34}, D_{35}, and D_{36}. Inconsistent model with respect to energy, consistent with respect to vorticity.

Model IV: All the terms denoted by A_{mn}, B_{mn} and D_{mn}. Inconsistent model with respect to energy, consistent with respect to vorticity.

As we can see, Model I corresponds to the ordinarily two-parameter model with constant static stability, CHARNEY, PHILLIPS (1953). This model is energetically consistent with the quasi-geostrophic approximation.

It must be pointed out that this is only valid if we let "f" be a variable in (2.13) and (2.14). Multiplying eqs. (2.8) and (2.9) with ψ^m and ψ^d respectively and then adding the change of the kinetic energy, can be written in the following average way:

$$\frac{\partial \bar{K}}{\partial t} = \frac{p_0}{g}\Big[\overline{\psi^m J(\psi^m,\eta^m)} + \overline{\psi^m J(\psi^d,\xi^d)} + \overline{\psi^d J(\psi^d,\eta^m)} + \overline{\psi^d J(\psi^m,\xi^d)} - \frac{p_0}{g\Delta p}\overline{\psi^d f\omega}\Big] = \frac{p_0}{g}\big[\overline{\tfrac{1}{2}J(\psi^{m2},\eta^m)}$$

TABLE 1

	Kinetic energy	Gross static stability	Kinetic energy	Gross static stability	Ratio between the change in kinetic energy and gross static stability
	Initial state		36-hour forecast		
Model II	4125	18182	5707	19740	1.01
Model III	4125	18182	5885	19719	1.14
Model IV	4125	18182	5958	19648	1.25

Units: kj/m^2.

$$+\tfrac{1}{2}\overline{J(\psi^{d2},\eta^m)}+\overline{J(\psi^m\psi^d,\xi^d)}-\overline{\psi^d f W}]. \tag{5.1}$$

The corresponding expression for the available potential energy reads:

$$\frac{\partial}{\partial t}\bar{A}=\frac{R\Delta p}{2^\varkappa g}\overline{\theta W}. \tag{5.2}$$

Where, as before, $(\overline{\quad})$ means an integration over a closed area.

Since an integration of a Jacobian over a closed area is zero it follows immediately from eqs. (5.1) and (5.2) that:

$$\overline{\psi^d f W}=\frac{R}{2^{\varkappa+1}g}\overline{\theta W} \tag{5.3}$$

if the total energy is conserved.

Further it is seen from eq. (2.9) that the vorticity of the thermal field is not conserved since the correlation between f and W is not necessarily zero. If we want to conserve the relative vorticity for the thermal field or the mean temperature, then f must be a constant. If f is constant in (2.9) (the term denoted A_{43}), then f must be a constant in (2.13) according to (5.3).

Let us qualitatively discuss what the effect will be if we use f instead of f_0. For an amplifying disturbance we often have a negative energy conversion in the meridional plane. This means that the warm air to the south is sinking and the cold air to the north is rising. The net effect of the term $-\overline{fW}$ will therefore be a slight increase in the mean temperature. In the experiment with Model I using $\gamma^d=\frac{1}{2}\pi$ the relative change for the stream function ψ^d was $+0.0005$ % for 36 hours which corresponds to an increase in the mean temperature of 0.1°K. Thus the effect of a variable f in Model I in this experiment is almost insignificant.

In Model II the static stability is allowed to vary, thus we can describe the static stabilization accompanying the release of kinetic energy. This model corresponds to a model investigated by GATES (1961, 1963), and yet, we have here used the quasi-geostrophic approximation. The terms denoted A_{mn} and B_{mn} are consistent with the quasi-geostrophic approximation, whereby this model also is energetically consistent.

In Model III we also include, in the equation for the mean flow, the vertical advection of vorticity, the twisting effect, the advection of vorticity by the divergent wind and the divergence term depending on the relative vorticity.

Together with the term included in Model III, in Model IV we also consider the divergence term depending on the relative vorticity in the thermal flow.

Both Models III and IV are *consistent regarding the conservation of vorticity,*

$$\text{since}\qquad \overline{\frac{\partial\xi^m}{\partial t}}=0 \quad\text{and}\quad \overline{\frac{\partial\xi^d}{\partial t}}=0.$$

However, these models are *inconsistent regarding the conservation of the total energy,* since we are only using the quasi-geostrophic approximation. It may be of interest to see if this inconsistency is significant or not.

In this first experiment we shall compare the results from Models II, III, and IV. The initial fields have the form:

$$\psi^m=-U^m y+\psi^m_A\sin\frac{2\pi}{L}x\cos\frac{2\pi}{D}y+\psi^m_0, \tag{5.4}$$

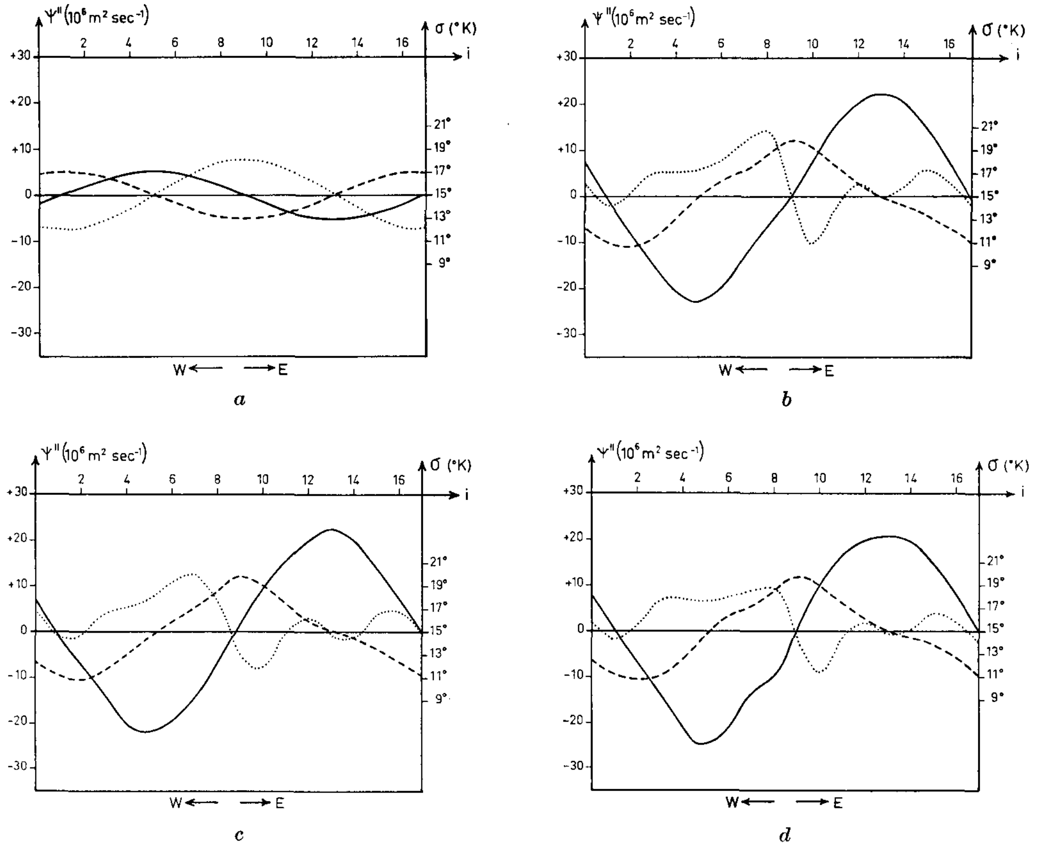

FIG. 4. The variation of the stream-function for the mean field, ψ^m (solid line), the stream-function for the thermal field, ψ^d (dashed line) and the static stability (dotted line) in the middle of the channel ($j=0$). (*a*) Initial state, (*b*) 36-hour forecast with Model II, (*c*) 36-hour forecast with Model III and (*d*) 36-hour forecast with Model IV.

$$\psi^d = -U^d y + \psi^d_A \sin \frac{2\pi}{L}(x-\gamma^d) \cos \frac{2\pi}{D} y + \psi^d_0, \tag{5.5}$$

$$\sigma = \sigma_0 + \sigma_A \sin \frac{2\pi}{L}(x-\gamma^s) \cos \frac{2\pi}{D} y, \tag{5.6}$$

where

$U^m = 25$ m sec^{-1}	$L = 4800$ km
$U^d = 15$ m sec^{-1}	$D = 3600$ km
$\sigma^0 = 15°$C	$\gamma^d = \frac{1}{2}\pi$
$\psi^m_A = 50 \cdot 10^5$ m^2 sec^{-1}	$\gamma^s = \frac{1}{2}\pi$
$\psi^d_A = 50 \cdot 10^5$ m^2 sec^{-1}	$\psi^m_0 = 5500 \cdot 10^5$ m^2 sec^{-1}
$\sigma_A = 3°$C	$\psi^d_0 = 3500 \cdot 10^5$ m^2 sec^{-1}

The amplitude for the static stability field as well as the phase difference between the mean and static stability fields have been given the values above in order to agree roughly with the values found by WIIN-NIELSEN (1963). He found that the perturbation stability is about 20 % and the corresponding γ^s 110° for an unstable wave. The time-integration of the systems (2.17)–(2.20) has been performed for 36 hours.

Figs. 5, 6, and 7 show the variation of the total kinetic energy and the gross static stability for Models II, III, and IV respectively. We see that the conservation of the difference between the kinetic energy and the gross static stability is very good for the consistent model, but for the two others the kinetic energy of the baroclinic disturbance is increasing more than the gross static stability.

It is seen in Table 1 that for Model IV the increase in the kinetic energy is surpassing the increase in the gross static stability by 25 %. This means that the effect of the inconsistency in Models III and IV as compared with the quasi-geostrophic assumption is rather serious and the ultimate effect of the static stabilization may be cancelled.

Fig. 4 shows in a cross section along the middle of the channel ($j = 0$) the initial waves for the mean field, thermal field, and the static stability (*a*) as well as the state after 36 hours for Models II (*b*), III (*c*), and IV (*d*). The forecasts show no significant differences, the troughs and the ridges have for example almost the same positions. The mean static stability is somewhat higher in Model II, but the amplitudes are also almost the same in the three models. The greatest differences are found in the meridional plane, and in the zonal kinetic energy.

6. The effect of an energy conservative Jacobian operator in short-time forecasts

The difference expression (A. 9) which corresponds to the Jacobian operator has the property of conserving the total kinetic energy for the barotropic model. As can be seen in the appendix this depends on a consistent truncation of differential expressions of the kind $\alpha](\alpha_1\beta)$

Since a model which is consistently formulated in the differential version conserves the total energy very well we can say without performing any special experiments that the usual difference expression is satisfying enough for short periodic forecasts. Yet, it may be interesting to see to what degree the use of (A. 9) instead of (A. 8) will improve the conservation of the total energy in a two-layer model.

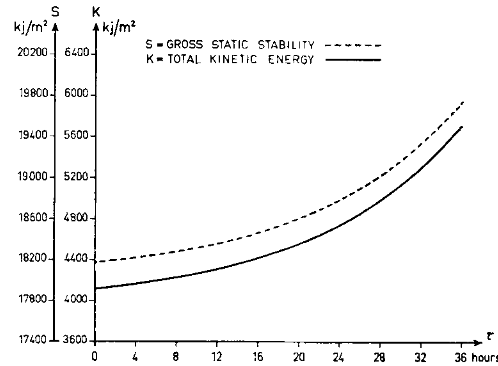

FIG. 5. The variation of total kinetic energy (solid curve) and gross static stability (dashed curve) with time in kj/m². In order to simplify the comparison, the curves have been placed together. The y-axis to the left refers to the gross static stability and the y-axis to the right to the total kinetic energy. Model II.

The result of such a comparison is given in Table 2. This table shows the total kinetic energy, the gross static stability and the difference between the change over one time-step for the kinetic energy and the gross static stability. As we can see from the total difference (in the bottom of the table) this difference is significantly smaller if we use $\mathbf{J}'(\alpha, \beta)$. For short-time routine forecasts, however, the improvement may be of little practical value.

We will further investigate how an energy conservative Jacobian operator will influence the wave-speed. To simplify the problem as much as possible we will restrict ourselves to barotropic waves moving in a β-plane.

The barotropic equation reads:

$$\frac{\partial \xi}{\partial t} = -\mathbf{J}(\psi, \eta) \tag{6.1}$$

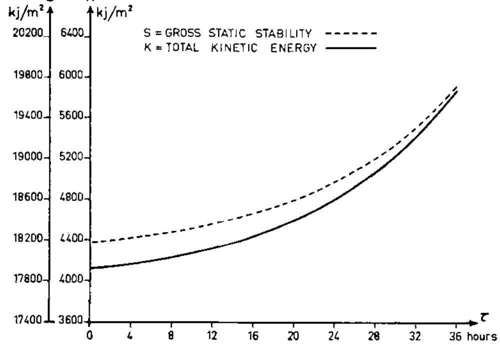

FIG. 6. The same as for Fig. 5 but with Model III.

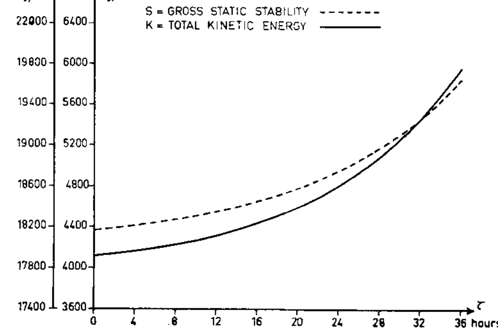

FIG. 7. The same as for Fig. 6 but with Model IV.

TABLE 2. *The change of total kinetic energy (K) and gross static stability (S) with time (τ). Units: kj/m². For further explanation see text.*

Conventional Jacobian operator				Energy-consistent Jacobian operator			
τ	K	S	$\Delta K - \Delta S$	τ	K	S	$\Delta K - \Delta S$
½	6731	29573		½	6729	29572	
1	6821	29682	−19	1	6818	29679	−18
2	7046	29901	+ 6	2	7040	29895	+ 6
3	7276	30127	+ 4	3	7267	30117	+ 5
4	7505	30351	+ 5	4	7493	30336	+ 7
5	7718	30565	− 1	5	7703	30543	+ 3
6	7913	30761	− 1	6	7899	30732	+ 7
7	8083	30938	− 2	7	8065	30896	+ 2
8	8218	31074	− 6	8	8203	31029	+ 5
9	8323	31183	− 4	9	8309	31128	+ 7
10	8386	31254	− 8	10	8371	31189	+ 1
11	8412	31287	− 7	11	8405	31212	+11
12	8399	31281	− 7	12	8387	31195	− 1
13	8347	31237	− 8	13	8346	31143	+11
14	8263	31158	− 5	14	8262	31053	+ 6
15	8142	31044	− 7	15	8148	30934	+ 5
16	7998	30904	− 4	16	8010	30786	+10
17	7829	30740	− 5	17	7843	30618	+ 1
18	7640	30559	− 8	18	7664	30433	+ 6
19	7445	30364	± 0	19	7469	30239	− 1
20	7237	30166	−10	20	7271	30040	+ 1
21	7036	29969	− 4	21	7074	29845	− 2
22	6835	29777	− 9	22	6880	29656	− 5
23	6651	29602	− 9	23	6703	29482	− 3
24	6480	29440	− 9	24	6535	29323	− 9
	Change for 24 hours −118				Change for 24 hours +55		

and the waves have the form:

$$\psi' = \psi_A \sin \frac{2\pi}{L}(x - ct) \cos \frac{2\pi}{D} y. \tag{6.2}$$

In order to compute the operators we must replace our continuous variables with discrete ones:

$$x = i\Delta s, \quad y = j\Delta s, \quad t = t\Delta t,$$

$$L = L_x \Delta s, \quad D = L_y \Delta s$$

when $0 \leqslant i \leqslant L$ and $-M \leqslant j \leqslant +M$.

L_x and L_y are integers which had to be multiplied with the grid-length in order to give the zonal and meridional wave-lengths respectively.

Since the waves will keep their amplitude constant in this experiment we will get an expression for the ratio (r) between the finite-difference wave-speeds if we compute the ratio between the Jacobian operators. Thus:

$$r = \frac{\mathbf{J}'(\psi,\eta)}{\mathbf{J}(\psi,\eta)}, \tag{6.3}$$

where

$$\psi = Uj\Delta s + \psi_A \sin \frac{2\pi}{L_x}\left(i - c\tau \frac{\Delta t}{\Delta s}\right) \cos \frac{2\pi}{L_y} j + \psi_0. \tag{6.4}$$

$\mathbf{J}(\alpha,\beta)$ and $\mathbf{J}'(\alpha,\beta)$ are then computed for an arbitrary point at $\tau = 0$.

After some calculations we get:

$$\mathbf{J}(\psi,\eta) = -4\psi_A \cos \frac{2\pi}{L_x} i \cos \frac{2\pi}{L_y} j \sin \frac{2\pi}{L_x} (\beta^2 - k^2 U), \tag{6.5}$$

$$\mathbf{J}'(\psi,\eta) = -4\psi_A \cos \frac{2\pi}{L_x} i \cos \frac{2\pi}{L_y} j \sin \frac{2\pi}{L_x} \times (\beta - k^2 U) \frac{2 + \cos \dfrac{2\pi}{L_y}}{3}, \tag{6.6}$$

where k is the wave-number

and for the ratio:

$$r = \frac{U - \frac{\beta}{k^2}\left(\frac{2+\cos\frac{2\pi}{L_y}}{3}\right)}{U - \frac{\beta}{k^2}} = \frac{2+\cos\frac{2\pi}{L_y}}{3}. \quad (6.7)$$

Consequently we have found that the ratio is a function of the meridional wave-length; and it follows that the waves are propagated slower if we use an energy consistent Jacobian operator. Yet, this effect is only observed for waves with small meridional extension or for large grid-lengths. In this connection "meridional" must be interpreted as the direction perpendicular to the direction of the basic flow.

Fig. 8 shows the wave-speed for the Jacobian operators (A. 8) and (A. 9) as compared with the analytical wave-speed. The result presented in the figure is obtained from a numerical integration for the channel model (see appendix and Fig. 3). The initial state is given by (6.2).

The numerical values used here have been somewhat different from those in the other sections. Thus, $L = 2400$ km and $\psi_A = 10^7$ m² sec⁻¹.

The curves in Fig. 8 exhibit some interesting features.

The error in the wave-speed which we get if we use the ordinary Jacobian operator (curve b) is rather small and changes very little with increasing meridional wave length. As was indicated in (6.6) the wave-speed which corresponds to the energy consistent operator is quite different (curve c) when L_y is very small.

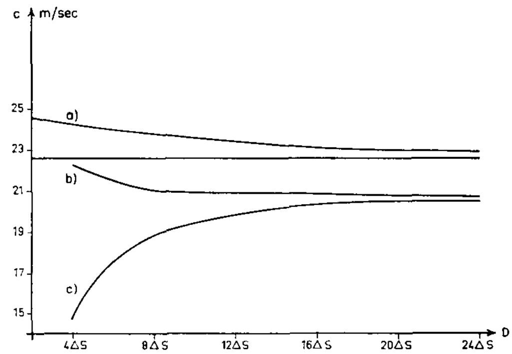

FIG. 8. The wave-speed in a barotropic model as a function of the meridional wave-number for different finite-difference schemes: (a) Analytical wavespeed. (b) Ordinary difference operator for the Jacobian operator. (c) Energy-consistent Jacobian operator. The basic velocity is 25 m sec^{-1} and the zonal wavelength 2400 km.

7. The structure of waves in two-level models with constant and variable static stability

In this section we will make some comparisons between the behaviour of baroclinic waves for Model I and Model II.

The ordinary two-level model has, as was pointed out in the introduction, a pronounced tendency to overpredict the kinetic energy. This is especially true in connection with intensive cyclone developments and the real reason for this misbehaviour is obscure. The purpose of the experiment, described in this section, is to answer the question whether a model with variable static stability could conceivably suppress a baroclinic development.

Before we start the discussion let us briefly describe the history of a wave disturbance as we observe it on the weather map. In the initial state the axis of the disturbances is sloping towards the "cold" side indicating that the temperature wave is lagging behind the pressure wave. During the development stage (a process of 12–24 hours) the temperature wave is catching up the pressure wave and in the mature stage the disturbance is almost quasi-barotropic. Hereafter the disturbance starts to decay mainly as the consequence of the frictional dissipation and the time-scale of this process is of the order 2–5 days. It seems very natural to assume from the empirical point of view that *adiabatic* processes may describe the transformation from a baroclinic to a quasi-barotropic state but *diabatic* effects may account for the development from the quasi-barotropic to the baroclinic state. However, the author is not aware of any synoptic investigation where this process has been studied systematically, but the remarkably good forecasts with the barotropic model from a quasi-barotropic initial state in areas where diabatic sources and sinks are unimportant, strongly suggest the conservation of the quasi-barotropic state within an adiabatic and a frictionless atmosphere.

This problem has been discussed by THOMPSON (1959) who showed that the local change of total rotationality and occlusion (defined in section 5) depends on the initial phase difference between the mean and thermal fields. If γ^d is situated in the interval $0, \pi$ (the temperature

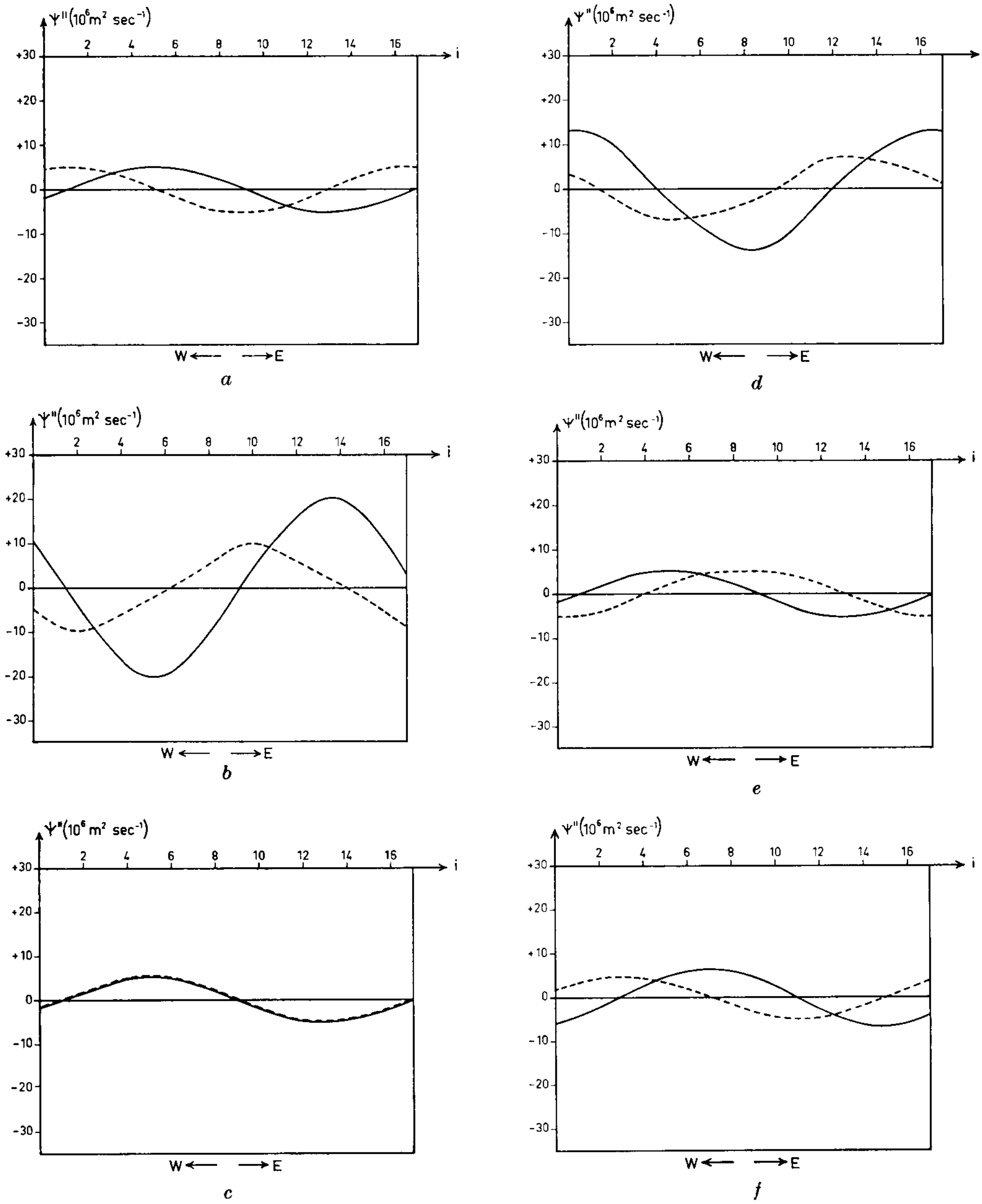

FIG. 9. The variation of the stream-function for the mean field, ψ^m (solid line), the stream-function for the thermal field, ψ^d (dashed line) in the middle of the channel. Model I. (*a*) Initial state, the phase-difference between the mean and thermal field ($\gamma^d = \frac{1}{2}\pi$). (*b*) 36-hour forecast with the initial fields (*a*). (*c*) Initial state ($\gamma^d = 0$). (*d*) 36-hour forecast with the initial fields (*c*). (*e*) Initial state ($\gamma^d = -\frac{1}{2}\pi$). (*f*) 36-hour forecast with the initial fields (*e*).

wave is lagging behind the pressure wave) the rotationality will increase and for γ^d in the interval $-\pi, 0$ the rotationality will decrease. For $\gamma^d = 0, \pm\pi$ the rotationality will be constant.

However, these results differ from those obtained by OGURA (1957) who found that for the amplifying unstable baroclinic wave the phase difference, γ^d, has a positive, limiting

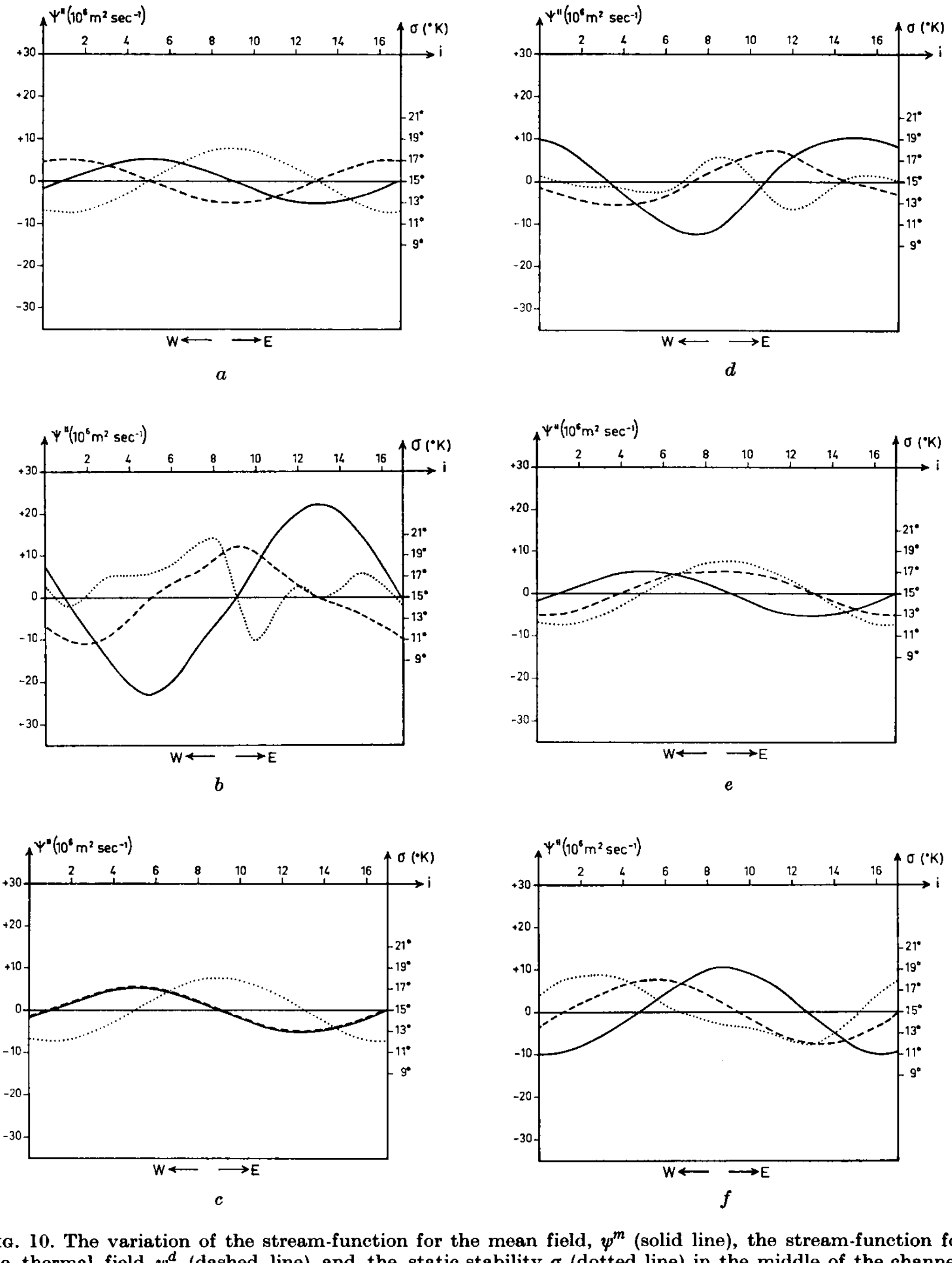

FIG. 10. The variation of the stream-function for the mean field, ψ^m (solid line), the stream-function for the thermal field ψ^d (dashed line) and the static stability σ (dotted line) in the middle of the channel. Model II. (*a*) Initial state, the phase difference between the mean and thermal field ($\gamma^d = \frac{1}{2}\pi$). (*b*) 36-hour forecast with the initial fields (*a*). The same figure as 4*a* and 4*b*. (*c*) Initial state ($\gamma^d = 0$). (*d*) 36-hour forecast with the initial fields (*c*). (*e*) Initial state ($\gamma^d = -\frac{1}{2}\pi$). (*f*) 36-hour forecast with the initial fields (*e*).

value which is independent of the initial phase difference. Any unstable wave will therefore ultimately get a positive phase lag, and the amplitudes will after a certain time start to grow. For the stable waves the phase lag will pass through all possible values giving a fluctuating amplitude to the disturbance.

Since the results by Ogura were obtained by a linearized treatment of the dynamic equations it may be interesting to see what the result will be if we perform a numerical experiment, where we can also consider the non-linear terms, that is, the interaction between the basic stream and the disturbance. In this experiment we have used Model I and Model II since we also want to study the effect of a variable static stability. Figs. 9*a*, 9*c* and 9*e* show the initial states (analytically given in section 5) for $\gamma^d \frac{1}{2}\pi$, 0 and $-\frac{1}{2}\pi$ respectively, and 9*b*, 9*d* and 9*f* show the corresponding 36-hour forecasts. The amplitudes are largest in the case where the initial temperature wave had a positive phase lag and smallest where the initial temperature wave had a negative phase lag.

On the other hand the phase lag has the value $3\pi/8 \pm \pi/8$ in the three cases, indicating that in this experiment also the phase lag is approaching a limiting value.

Concerning Model I we may compare our result with Ogura's computations. With our notations his expression for the phase lag, γ, reads:

$$\gamma = tg^{-1}\left(-\frac{iF}{2kU^d}\right),$$

where

$$F = \left[2u^d(k^2-4) + \frac{1}{4\pi^4}\left(\frac{\beta L^2 D^2}{L^2+D^2}\right)^2\right]^{\frac{1}{2}},$$

$$K = \frac{4\pi^2(L^2+D^2)}{f_0^2 L^2 D^2}\,\frac{2^{\varkappa+1}}{R}\,\frac{1}{\sigma_0}$$

and $$i = \sqrt{-1}.$$

During the development the meridional wavelength D increased to 7200 km which, together with the value presented in section 5, gives $\gamma = 30°$. This value is smaller than those found in the experiment. The difference may be due to interaction between the basic flow and the wave or to numerical approximations.

The behaviour of the waves in an atmosphere with a variable static stability may be studied in Fig. 10. (*a*), (*c*), and (*e*) show the three initial states for $\gamma^d = \frac{1}{2}\pi, 0$, and $-\frac{1}{2}\pi$ and (*b*), (*d*), and (*f*) show the corresponding 36-hour forecasts. If we first disregard the forecasts of static stability, we see when we compare the results from Models I and II that the forecast of pressure and temperature waves differs somewhat in amplitude and position. The real wave-speed has become somewhat smaller in Model II, but the imaginary part of the wave-speed is larger for this Model, indicated by the larger amplitudes. This last statement is more easily verified in Fig. 11, where we have plotted the total kinetic energy of the disturbance as a logarithmic function of time for the three initial states. During the very first hours the waves behave as proposed by THOMPSON (1959), but after less than 16 hours all waves have started to amplify.

After the next hours the perturbation energy increases almost exponentially for all the curves and the rate of amplification is almost independent of the initial state. (For Model I the perturbation kinetic energy doubles every 6 hours on the average and for Model II for every 5 hours.) The *e*-folding times given from the linear theory (GATES (1961)) agree roughly with these values. The limiting phase lag γ^d is almost the same as for Model I.

The difference between Models I and II is very small in the cases where the initial phase lag is $\frac{1}{2}\pi$, but it is more pronounced when $\gamma^d = 0$ and $-\frac{1}{2}\pi$, and thus when the rate of amplification is small.

The reason for this is associated with the fact that the initial phase lag for the stability wave, γ^s, has been the same in all the three cases. Since the contribution from the terms denoted B_{mn} on the whole is smaller than from the terms denoted A_{mn} they will be greatly surpassed when the waves have reached their maximum development rate. On the other hand when the contribution from A_{mn} is small the effect from B_{mn} is observed and the effect may be different depending on the prescribed initial state.

For the matter of the static stability some details will be pointed out. In the initial state the most stable air is found in front of the ridge but in the forecasts the most stable air is found over and just in front of the trough. Since also an unstable area is found just in front of the temperature ridge the static stability field exhibits a very small scale appearance. We will discuss qualitatively the large gradient in the static stability just over the temperature ridge. For the most effective release of kinetic energy the temperature and vertical velocity are correlated in such a way that the warm air is rising and the cold air is sinking. This correlation is very well established in this experiment. From the continuity equation it then follows that the divergence will be distributed with low and level convergence under the mean level temperature trough. If we now examine the term in the stability equation which dynamically describes the variation of the static stability, namely $f\nabla\psi^d \cdot \nabla\chi$ we will get a positive contribution behind the temperature ridge and a negative contribution in front of the temperature ridge.

Since for an amplifying disturbance the temperature wave is lagging behind the pressure wave with a phase lag of between $\frac{1}{2}\pi$ and $\frac{1}{4}\pi$ we will on an average get a stabilizing effect over the troughs and an instabilization over the ridges (Figs. 10*b*, *d*, and *f*).

It is further seen from the forecasted static stability that the stability is greatly broken up. The reason for this is perhaps that the advective term $J(\psi^m, s)$ and the dynamic terms $f\nabla\psi^d \cdot \nabla\chi$ in the eq. (2.19) may work somewhat independent of each other giving rise to smaller scale static stability variations.

8. Energy transformations

Let us now make a more detailed investigation of Models I and II. We will also perform some comparisons with the result presented by Gates (1963) who has integrated models very similar to Models I and II over the whole northern hemisphere. Since the atmosphere is quasi-barotropic over large areas, it is natural to choose for the comparisons the case when the temperature wave and the pressure wave are in phase.

The integrals defined in section 5 have been computed at every time-step and they are depicted in Fig. 12.

Some details in the figures may be discussed. Let us start from the energy transformation from the available potential energy to the kinetic energy, $\{A, K\}$. As to the eddy transformation, Model I has continually a positive conversion resulting in a monotonous increase

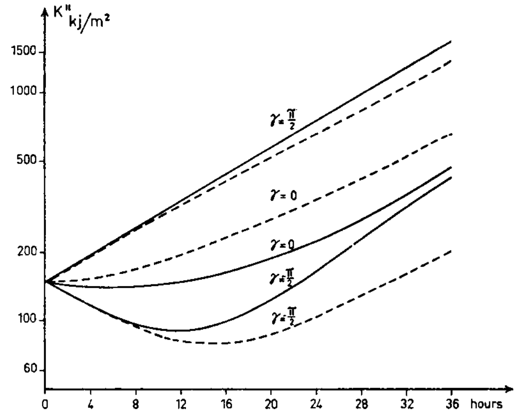

Fig. 11. The total perturbation kinetic energy as a function of time in unstable baroclinic waves from various initial conditions. Solid curves indicate a two-level model with variable static stability and dashed curves a two-level model with constant static stability.

in the eddy kinetic energy. For Model II we have on the contrary a reverse transformation during the first 8 hours (Fig. 12*e*), resulting in a reduction in the eddy kinetic energy during the same time (Fig. 12*a*). This is especially valid for the thermal part, $K^{d''}$. Also, the available potential energy has a correspondingly reversed variation (Fig. 12*d*). For Model II we have a general net transfer from the eddy available potential energy, A'', to the zonal available potential energy during the first part of the time integration. For Model I no such net transfer is observed.

It may also be pointed out that in the experiment which corresponds to the initial value $\gamma^d = \frac{1}{2}\pi$ no qualitative differences in the development were observed.

However, after 12 hours' integration the damping effect from the variation of the static stability becomes less pronounced and the behaviour of the waves in the two models is rather similar. The reason for this is the increasing effect from the baroclinic terms demonstrated by the change in the phase difference between the pressure and temperature wave. The phase lag increases more and more as it approaches a limiting value.

Fig. 12*f* shows the variation of occlusion and total rotationality with time. The occlusion, as it has been defined here, is a semi-correlation between the mean and thermal fields. The

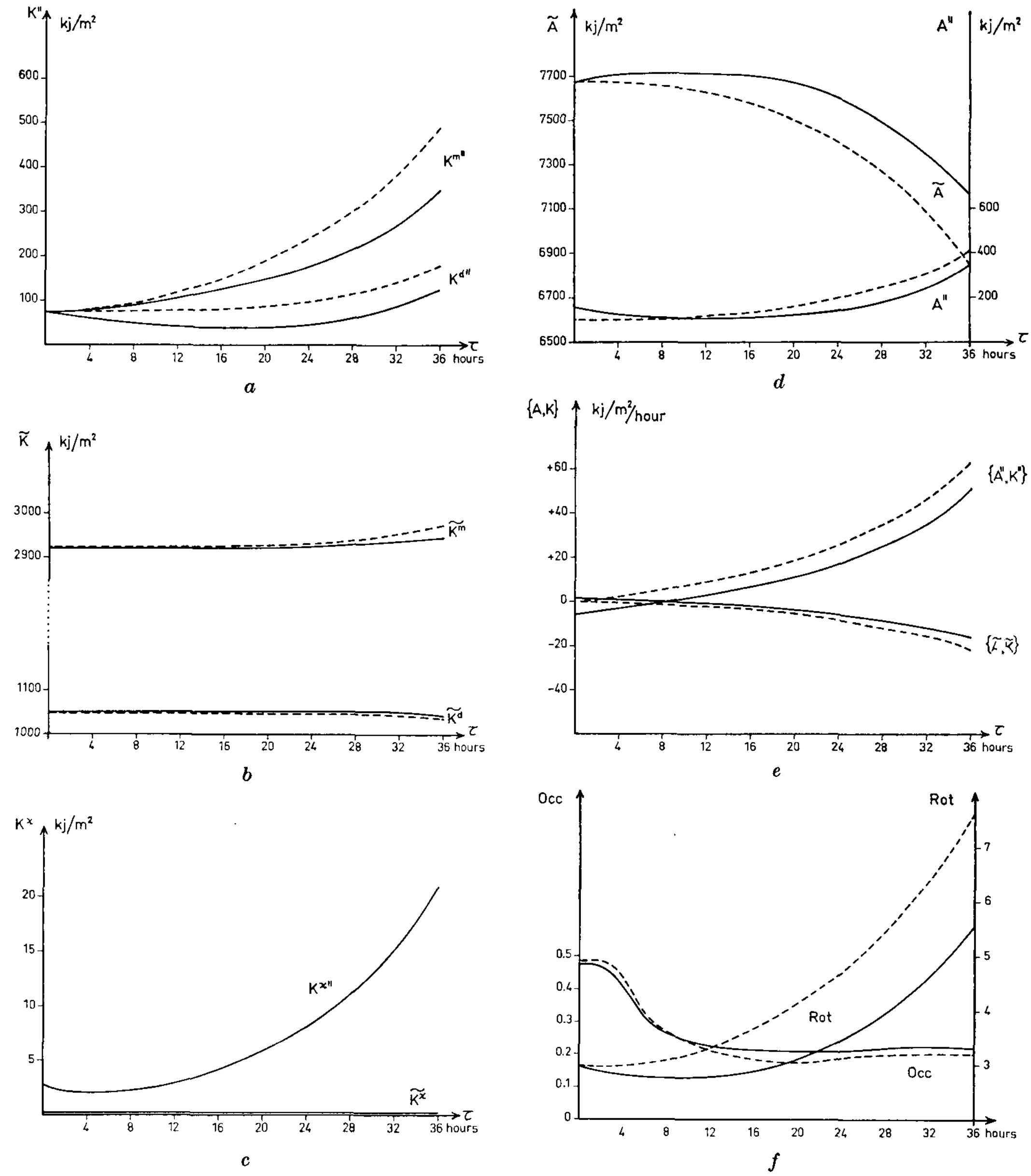

FIG. 12. Dashed lines refer to Model I (constant stability) and solid lines to Model II (variable stability). (*a*) shows the variation of $K^{m''}$ and $K^{d''}$ with time; (*b*) the variation of $\widetilde{K^m}$ and $\widetilde{K^d}$; (*c*) the variation of K^χ and $K^{\chi''}$; (*d*) the variation of $\tilde{A}$ and A''; (*e*) the variation of $\{A'', K''\}$ and $\{\tilde{A}, \tilde{K}\}$ and (*f*) the change of occlusion and total rotationality. For further explanations, see text.

change in occlusion will only roughly accompany the change in the phase difference, and so the curve in the figure has been somewhat smoothed. The occlusion and the total rotationality is almost constant during the very first hours implying that the results obtained by THOMPSON (1959) are only valid during the first 2–4 hours. After this the occlusion changes rapidly, whereupon it gradually assumes another constant value. The change in the occlusion is almost the same for Models I and II and the variation of the static stability will not change the limiting phase difference. The variation of the total rotationality shows a somewhat different appearance. In this case the static stability is causing a delay in the development of the rotationality. Considered from the initial state after 8 hours the development in Model II is very similar to that in Model I. This "mechanism of delay" is also the general impression gained from Figs. 12*a*, 12*d*, and 12*e*. This is later compensated by a larger rate of amplification.

The result presented in this section is completely different from those given by GATES (1963). It is naturally difficult to draw any definite conclusions since the initial data and the area of integration are so different from this experiment. However, we are studying one of the most dominating wave-lengths of the atmosphere and the results given here for the energy transformations (Model I) also agree qualitatively with those given by WHITE & SALZMAN (1956) and WIIN-NIELSEN (1959) obtained from actual data. For example the ratio between $\{A'', K''\}$ and $\{\tilde{A}, \tilde{K}\}$ (which may be natural to regard as a measure of the scale of the energy processes) given by White and Salzman was 3:4, which agrees very well with our values (Fig. 12*e*).

Gates' values which correspond to Model II seem to be dubious. The transformation $\{K'', \tilde{K}\}$ is negative and reverse compared with Model I and the energy transformation $\{\tilde{A}, \tilde{K}\}$ is one order of magnitude larger in Model II than in Model I. In all our experiments the difference in $\{\tilde{A}, \tilde{K}\}$ between Model I and Model II is rather small (Fig. 12*e*).

9. Conclusions

We may summarize the result of this investigation in the following way:.

1. There is an obvious indication that the phase difference γ^d is approaching a limiting value for both Model I and Model II independent of the initial phase difference. This remark is a very important one and reflects a serious misbehaviour of the two-level model. As we have seen, the two-layer model does not conserve the quasi-barotropic state ($\gamma^d = 0$) but gives rise very soon to a baroclinic development. Other experiments, with more realistic, zonal wind-profiles show the same kind of behaviour.

We can conclude that a very reasonable explanation for the erroneous increase in the kinetic energy and the incapability to predict the subsequent development of mature disturbances is due to the property of the two-level model of creating amplifying baroclinic states, independent of the initial arrangement of temperature and pressure (height).

2. The phase difference γ^s also seems to approach a limiting value manifested by a stabilization of the troughs and an instabilization of the ridges.

3. Models which are physically inconsistent with respect to the energy transformations give rise to rather serious errors within 36 hours which may account for spurious sources of kinetic energy.

4. The improvements in the conservation of the total energy which depend on the use of an energy-consistent difference form of the Jacobian operator are very small, and may be insignificant with respect to actual data. The use of this operator implies furthermore that the truncation error will increase for small meridional wave-lengths. This is manifested by a significant decrease in the finite-difference wave-speed. The error arising from the ordinary Jacobian operator is much smaller, and for sufficient large wave-lengths in the zonal direction the difference between the analytical- and the finite-difference wave-speed changes rather little. An experiment with actual data verified this.

5. The effect of the variation of the static stability and of the divergent part of the wind is largest during the first 12 hours and we may get a *qualitatively* different behaviour between Model I and Model II. After this the baroclinic terms increasingly dominate the development and after 24 hours Model II behaves in the same way as Model I. The *quantitative* differences are characterized by a slower wave-speed for Model II and a larger amplification rate (about 15 %) when the development has started. The energy transformations are on the whole very similar to those for Model I.

The stabilization following the increase of the kinetic energy will conceivably not break the development, but we will get instead too large an increase in the static stability since the difference between the total kinetic energy and the gross static stability is an invariant. If one is interested in large scale static stability forecasts, say, as a basic predictor to thunderstorm forecasts, the best thing is evidently to eliminate the term in the equation for the static stability which describes the dynamical changes after 12 or 24 hours, depending on the smooht-ing and the grid-length.

The same may be said about the baroclinic term in the equation for the mean field. This last interference has also been done at some forecasting centres in order to improve the routine baroclinic forecasts. As is seen from Fig. 11 this is mostly consistent with respect to the errors of the model.

To get a conception of the applicability of the result from the channel experiment the models have also been tested with respect to real data. The case which was tested was characterized by a high baroclinicity ($\gamma^d \sim \frac{1}{2}\pi$) which gave a large amplification rate. The result of the forecast justified the channel experiment; thus we get only slight quantitative differences with a larger amplitude and slower wave-speed in Model II than in Model I.

As we have found in this investigation a variable static stability will not suppress the release of kinetic energy. The lack of variable static stability in a two-layer model is therefore not the primary reason for the errors in prediction. Since we have also in this experiment eliminated the errors depending on improper side-boundary conditions we may highly suspect the "geometrical" constraints on the three-dimensional windfield depending on the lack of vertical resolution.

Acknowledgements

The author wishes to express his thanks to Prof. B. Bolin and to Dr. B. Döös for many helpful and constructive suggestions and stimulating discussions throughout this work. He also wishes to thank the other members of the section for research in numerical weather-forecasting at the Swedish Meteorological and Hydrological Institute.

REFERENCES

DÖÖS, B. R., 1962, Routine numerical weather prediction in Sweden. *Proceedings of the International Symposium on Numerical Weather Prediction in Tokyo*, Meteorological Society of Japan, Tokyo, pp. 21–23.

GATES, W. L., 1961, The stability properties and energy transformations of the two-layer model of variable static stability. *Tellus*, **13**, pp. 460–471.

GATES, W. L., and C. A. RIEGEL, 1963, Comparative numerical integration of simple atmospheric models on a spherical grid. *Tellus*, **15**, pp. 405–423.

LORENZ, E. N., 1960, Energy and numerical weather prediction. *Tellus*, **12**, pp. 364–373.

OGURA, Y., 1957, Wave solutions of the vorticity equation for the 2½-dimensional model. *Journal of Meteorology* **14**, pp. 60–64.

THOMPSON, P. D., 1959, Some statistical aspects of the dynamical processes of growth and occlusions in simple baroclinic models. *The Rossby Memorial Volume*, Stockholm 1959, pp. 350–358.

WHITE, R. M., and SALZMAN, B., 1956, On the conversion between potential and kinetic energy in the atmosphere. *Tellus* **8**, pp. 357–363.

WIIN-NIELSEN, A. C., 1959, A study of energy conversion and meridional circulation for the large-scale motion in the atmosphere. *Monthly Weather Review*, vol. **87**, pp. 319–332.

WIIN-NIELSEN, A. C., 1960, A note on the thermal structure of waves in a simple baroclinic model, *Technical memorandum no.* **17** *Joint numerical weather prediction unit national meteorological center*. Washington, D. C.

WIIN-NIELSEN, A. C., 1963, On baroclinic instability in filtered and non-filtered numerical prediction models. *Tellus*, **15**, pp. 1–19.

Appendix

Finite-difference channel model

The numerical method of solution requires a space–time grid network and replacement of the continuous variables by grid variables defined only at the grid points. Thus we have:

$$x = i\Delta s, \quad y = j\Delta s, \quad t = \tau\Delta t,$$

where i, j and τ are the grid variables, Δs the grid-length and Δt the timestep.

The x-axis is oriented to the east and the y-axis to the north (see Fig. 3) and we consider an atmospheric section in the shape of a channel. The channel has walls to the north ($y = +M$) and to the south ($y = -M$), where the kinematic boundary condition requires the disappearance of the meridional wind component v.

In the zonal x-direction the channel is unlimited, but with all dependent variables and their derivatives cyclically continuous in x. Consequently for an arbitrary function α, the following identity is valid:

$$\frac{\partial^n}{\partial x^n}(\alpha) = \frac{\partial^n}{\partial x^n}(\alpha + L),$$

where L is the length of the channel. It suffices then to consider in the horizontal plane the rectangular area

$$0 \leqslant i \leqslant L, \quad -M \leqslant j \leqslant +M.$$

The numerical solution of the systems (2.17)–(2.19) was found from the approximating difference equations:

$$\nabla^2(\Delta_\tau \psi^m)_{ij} = \frac{\varepsilon \Delta t}{1}[\{A_{31}\mathbf{J}(\eta^m, \psi^m) + A_{32}\mathbf{J}(\xi^d, \psi^d)\} + \{(D_{33} + D_{36})W\nabla^2\psi^d + D_{34}\nabla W \nabla \psi^d + D_{35}\nabla \xi^d \nabla \chi\}]_{ij}, \quad \text{(A. 1)}$$

$$\left[\nabla^2 - \left\{\frac{A_{43}f + D_{45}\xi^m}{A_{12}s\mu}\right\}_{ij}\right](\Delta_\tau \psi^d)_{ij} = \frac{\varepsilon \Delta t}{1}\left[A_{41}\mathbf{J}(\xi^d, \psi^m) + A_{42}\mathbf{J}(\eta^m, \psi^d) + \frac{A_{43}f + D_{45}\xi^m}{A_{12}s}\{A_{11}f\mathbf{J}(\psi^m, \psi^d) + B_{13}\mathbf{J}(\psi^d, s) + B_{14}\nabla s \nabla \chi\} + B_{43}\nabla f \nabla \chi + D_{45}\nabla \xi \nabla \chi\right]_{ij}, \quad \text{(A. 2)}$$

$$\Delta_\tau s_{ij} = \frac{\varepsilon \Delta t \mu}{1}[B_{21}\mathbf{J}(\psi^m, s) + B_{22}f\nabla \psi^d \nabla \chi]_{ij}, \quad \text{(A. 3)}$$

$$\nabla^2 \chi_{ij} = \frac{1}{A_{12}s}\left[\frac{f\Delta_\tau \psi^d}{\varepsilon \Delta t \mu} + A_{11}f\mathbf{J}(\psi^m, \psi^d) + B_{13}\mathbf{J}(\psi^d, s) - B_{14}\nabla s \nabla \chi\right]_{ij}, \quad \text{(A. 4)}$$

$u = \left(\frac{m}{\Delta s}\right)^2$, where m is the map factor; $m = 1$ in the channel experiment. The finite-difference operators in the system (A. 1)–(A. 4) are defined in the following way (α and β stand for arbitrary variables):

$$\left(\frac{\partial \alpha}{\partial t}\right)_{ij} \simeq \frac{\Delta_\tau \alpha_{ij}}{\varepsilon \Delta t},$$

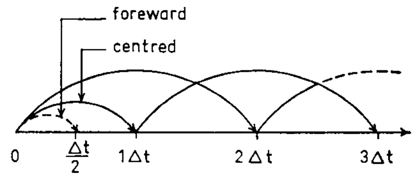

FIG. 2. Principles of the time integration. Solid line: forward time integration. Dashed lines: centered time integration.

where $\quad \Delta_\tau \alpha_{ij} = \alpha_{ij}^{\tau+1} - \alpha_{ij}^{\tau-1}$

and $\quad \varepsilon = 1 \quad \text{for} \quad \tau = \frac{1}{2},$

$$\varepsilon = 2 \quad \text{for} \quad \tau \geqslant 1. \quad \text{(A. 5)}$$

The time-integration is illustrated in Fig. 2.

$$(\nabla^2 \beta_{ij} = (\beta_{i+1,j} + \beta_{i-1,j} + \beta_{i,j+1} + \beta_{i,j-1} - 4\beta_{ij}), \quad \text{(A. 6)}$$

$$(\nabla \alpha \nabla \beta)_{ij} = \tfrac{1}{2}\{(\alpha_{i+1,j} - \alpha_{ij}) \cdot (\beta_{i+1,j} - \beta_{ij}) + (\alpha_{ij} - \alpha_{i-1,j}) \cdot (\beta_{ij} - \beta_{i-1,j}) + (\alpha_{i,j+1} - \alpha_{ij}) \cdot (\beta_{i,j+1} - \beta_{ij}) + (\alpha_{ij} - \alpha_{i,j-1}) \cdot (\beta_{ij} - \beta_{i,j-1}). \quad \text{(A. 7)}$$

It will be noted that the operator $(\nabla \alpha \nabla \beta)_{ij}$ had to be truncated in this way if we want to have a consistent finite difference form, analogues to the vector identity:

$$\nabla \cdot (\alpha \nabla \beta) = \nabla \alpha \cdot \beta + \alpha \nabla^2 \beta,$$

$$\mathbf{J}(\alpha_1 \beta)_{ij} = \tfrac{1}{4}\{(\alpha_{i+1,j} - \alpha_{i-1,j}) \cdot (\beta_{i,j+1} - \beta_{i,j-1}) - (\alpha_{i,j+1} - \alpha_{i,j-1})(\beta_{i+1,j} - \beta_{i-1,j})\}. \quad \text{(A. 8)}$$

It follows that

$$\sum_i \sum_j \mathbf{J}(\alpha_1 \beta)_{ij} \equiv 0$$

and $$\sum_i \sum_j \{\alpha_{ij}(\nabla^2 \beta)_{ij} + (\nabla \alpha \nabla \beta)_{ij}\} \equiv 0.$$

Thus, the total vorticity for the mean and thermal field separately is conserved in the difference equation if it is conserved in the differential equation.

It has been shown by LORENZ (1960) that a model including the terms noted A_{mn} and B_{mn}

combined with the balance criteria (2.13) conserves the sum of the available potential energy and kinetic energy and the difference between the gross static stability and kinetic energy. These energy invariants are not necessarily valid in the *difference* equation.

Recently Arakava (unpublished) has proposed a difference form of the Jacobian operator which implies that the kinetic energy is conserved in the one-dimensional barotropic model. The definition of this energy conservative Jacobian operator is:

$$\begin{aligned}\mathbf{J}'(\alpha_1\beta)_{ij} = \tfrac{1}{12}[&(\alpha_{i+1,j}-\alpha_{i-1,j})(\beta_{i,j+1}-\beta_{i,j-1}) \\ &-(\alpha_{i,j+1}-\alpha_{i,j-1})(\beta_{i+1,j}-\beta_{i-1,j})] \\ +\tfrac{1}{12}[&\{\alpha_{i+1,j}(\beta_{i+1,j+1}-\beta_{i+1,j-1}) \\ &-\alpha_{i-1,j}(\beta_{i-1,j+1}-\beta_{i-1,j-1})\} \\ &-\{\alpha_{i,j+1}(\beta_{i+1,j+1}-\beta_{i-1,j+1}) \\ &-\alpha_{i,j-1}(\beta_{i+1,j-1}-\beta_{i-1,j-1})\}] \\ +\tfrac{1}{12}[&\{\beta_{i,j+1}(\alpha_{i+1,j+1}-\alpha_{i-1,j+1}) \\ &-\beta_{i,j-1}(\alpha_{i+1,j-1}-\alpha_{i-1,j-1})\}] \\ &-\{\beta_{i+1,j}(\alpha_{i+1,j+1}-\alpha_{i+1,j-1}) \\ &-\beta_{i-1,j}(\alpha_{i-1,j+1}-\alpha_{i-1,j-1})\}].\end{aligned} \tag{A. 9}$$

The prime stands for the energy-conservative finite difference operator. Generally it follows that the use of (A. 9), together with appropriate boundary conditions implies that:

$$\sum_i\sum_j \alpha_{ij}\mathbf{J}'(\alpha,\beta)_{ij} \equiv \sum_i\sum_j \beta_{ij}\mathbf{J}'(\alpha,\beta)_{ij} \equiv \sum_i\sum_j \mathbf{J}'(\alpha,\beta)_{ij} \equiv 0$$

which is consistent with the corresponding differential operators.

Since in the energy transformations for the two-layer model we have also expressions of the kind $\alpha J(\alpha,\beta)$ see GATES (1961) we may get some improvement if we use $\mathbf{J}'(\alpha,\beta)$ instead of $\mathbf{J}(\alpha,\beta)$.